Available online at www.sciencedirect.com

ScienceDirect

Journal of Ocean Engineering and Science 5 (2020) 73–83

www.elsevier.com/locate/joes

Review Article

Design methodology of permanent magnet generators for fixed-pitch tidal turbines with overspeed power limitation strategy

Sofiane Djebarri[a], Jean Frédéric Charpentier[b], Frank Scuiller[b], Mohamed Benbouzid[c,d,*]

[a] ECAM Lyon, LabECAM, F69005 Lyon, France
[b] French Naval Academy, IRENav EA 3634, 29240 Brest, France
[c] University of Brest, UMR CNRS 6027 IRDL, 29238 Brest, France
[d] Shanghai Maritime University, 201306 Shanghai, China

Received 15 June 2019; received in revised form 3 September 2019; accepted 4 September 2019
Available online 10 September 2019

Abstract

This paper deals with a design methodology of permanent magnets (PM) generators used for fixed-pitch tidal turbines in a marine renewable energy context. In the case of underwater turbines, fixed-pitch tidal turbines could be very attractive and interesting to reduce maintenance operation by avoiding using such a complex electromechanical system for blade- pitching. In this technological case, one of the main control challenges is to ensure power limitation at high tidal current velocities. This control mode can be achieved using the generator flux-weakening. In this context, this paper proposes an original and systemic design methodology to optimize the generator design taking into account the tidal turbine power limitation for high tidal currents velocities.

Keywords: Tidal turbine; Fixed-pitch turbine; Direct-drive; PM generator; Design methodology; Flux-weakening power limitation.

1. Introduction

Tidal energy is a renewable source of energy with a potential easily predictable many years in advance [1]. This energy is due to the oceans currents that results from the gravitational moon and sun forces that act on the oceans and generates tides. When the tidal site is located in a narrow channel, the tides currents velocity are increased; to make the tidal site economically feasible the average value of the tides velocity should be higher than 2 m/s. In addition, tidal sites should be located near coasts and ports in order to make easier and cheaper tidal turbines implantation and connection to the electrical grid [2–4]. Considering hypothesis on the tidal sites and related technological solutions that can actually be utilized to extract energy form tides [5], the worldwide energy potential of this resource is estimated to 450 TWh/year. In Europe, the energy potential of tides is evaluated to 24 TWh/year and it is mainly located in UK and France, with respectively, 48% and 42% each one. Therefore, this energy could constitute a solution to complete the other renewable energy resources for power energy generation [1,2].

Marine current turbines (MCTs) are submerged under seawater and intended to extract energy from tidal currents [6]. Recent MCTs machines that are currently subject to industrial developments are quite similar in terms of the drivetrain to systems used in wind turbines [7]; these conversion chains can include the following elements:

- The turbine: according to the literature [7,8], horizontal axis turbines are mainly used in the first industrial MCTs prototypes. The turbines blades can include variable or fixed pitch systems [9–10]. The blades pitching mechanism allows to control the turbine power by varying the blades arrangement relative to the water flow of tides. However, this mechanical control system increases the complexity of

* Corresponding author at: University of Brest, UMR CNRS 6027 IRDL, 29238 Brest, France.
E-mail addresses: jean-frederic.charpentier@ecole-navale.fr (J.F. Charpentier), franck.scuiller@ecole-navale.fr (F. Scuiller), mohamed.benbouzid@univ-brest.fr (M. Benbouzid).

https://doi.org/10.1016/j.joes.2019.09.001

the tidal generation system and increases the failure probability of the MCTs [11,12]. Because of underwater offshore implantation of marine turbines, improving reliability and reducing maintenance will be key futures for sustainable and cost-attractive exploitation of marine tides.

- The gearbox: this mechanical element is incorporated in the drivetrain between the turbine shaft and the generator shaft. It permits to increase the shaft rotation speed of the generator. Geared solutions allow increasing the compactness of the generator even if they cause an important part of failures and maintenance needs [13]. In direct-drive system, the generator shaft is directly linked to the turbine shaft without including gearbox. This solution is attractive to reduce maintenance but due to low generator shaft speed it significantly increases the generator size, masse and cost [14].
- The generator: it realizes the energy conversion from mechanical to electrical energy. In direct-drive case, low speed permanent-magnet (PM) machines are mainly used. In this case, the rotational speed of the generator is typically below 50 rpm for high power turbines (MCTs) [15].
- The power converter: it allows controlling the operating point of the generator and permits the power regulation before injection to the grid. Several architectures of power converters can be possible according to the nature of utilized generator in the MCT system [16].
- The storage system: it is generally used for smoothing the electrical power before its injection into the electrical grid [17].

It can be noted that thanks to the fluid higher density (water has a density approximately 850 times higher than the air), tidal turbines are significantly more compact than wind turbines (for the same rated power), which appears as an economic advantage. [7]. However referring to [12] and the raised issue in [14], the gearbox and blade variable-pitch systems are the main sources of failure and maintenance in wind turbines. With tidal power turbines the maintenance is a key future because it is extremely difficult to perform maintenance operations on immersed seawater MCTs. In addition, the maintenance adds significant additional costs to the MCTs exploitation. In order to reduce maintenance requirements, a drivetrain simple architecture (with no gearbox and pitch control) can be a very attractive solution and has been adopted in several industrial projects [7]. This low maintenance drivetrain architecture is the solution that has been adopted in this study: a direct-drive radial flux PM generator driven by a fixed-pitch turbine (Fig. 1) [18].

Power limitation strategy is necessary to make a cost-attractive sizing of electrical energy conversion chain. By considering this strategy, a significant oversizing of the electrical drivetrain should be avoided. When the turbine has variable-pitch blades, blades pitching can mechanically achieve the power limitation strategy by changing the hydrodynamic forces on blades. This pitch control strategy is the most effective solution for MW size wind turbines. However in case of tidal turbines with a fixed-pitch configuration, the power limitation control has to be electrically carried out by the generator speed/frequency control (using the power converter) for under-speed or over-speed operations. For over-speed solution, a flux-weakening control strategy is used [9,19]. It consists in reducing the total generator flux by opposing the stator armature flux to magnets flux in order to decease the generator electromotive forces; when the generator shaft speed is very high. In this paper we propose a specific design methodology of a radial flux permanent magnets (RFPM) generator to perform the power limitation control strategy through only electrically controlling the RFPM generator. For that purpose, a systemic design approach of the PM generator is proposed [9,20]. Our methodology allows sizing the generator by considering the tidal site energy potential, the generator specifications, the turbine power coefficient (C_p) law, the converter voltage and power factor constraints and the generator power limitation strategy requirements. In the last part, a design is achieved according to the given methodology and the results are presented and discussed according to the generator operating speed cycle.

2. Design methodology

2.1. Tidal resource analysis

In this part, Raz de Sein, France, tidal site is considered for its high tidal currents velocity and its favorable location near the coasts. Tidal currents velocity profile data are used, these data gives the velocity values for each hour during 8424 h. These tidal currents speeds data are issued from French Oceanographic databases as described in [21]. Fig. 2 shows the velocity variation during the considered tidal currents window, while Fig. 3 gives the corresponding occurrences distribution during the tidal cycle (Fig. 2). The utilized data are given in Appendix.

The occurrences OCC_i is the number of hours corresponding to the ith tidal current velocity v_i, in the considered tidal window. Knowing tidal currents velocity occurrences allows calculating the corresponding kinetic energy of tides currents per m^2 (Wh/m^2). For each value of tidal current velocity the following formula is used:

$$E^i_{kinetic}(v_i) = \frac{1}{2}\rho_{water}\left|v_i^3\right| \times OCC_i(v_i) \quad (1)$$

where $E^i_{kinetic}$ is the kinetic energy given in (Wh/m^2) and ρ_{water} is the water density ($\rho_{water} = 995.6\,kg/m^3$ at 30 °C) and v_i is the tidal current velocity.

The tidal kinetic energy distribution, which is evaluated by (1) is shown in Fig. 4. It can be observed from this figure that the tidal kinetic energy distribution is close to two normal laws, one for the positive values of tidal current speed and another one for the negative values.

If kinetic energy per m^2 of the tidal site is known for each current speed value (v_i), it is then possible to deduce the extractible energy ($E^i(v_i)$) that can be harnessed by a marine turbine characterized by its swept blade area ($A_{turbine}$) and its maximum power coefficient (C_{pmax}). This calculation setup is

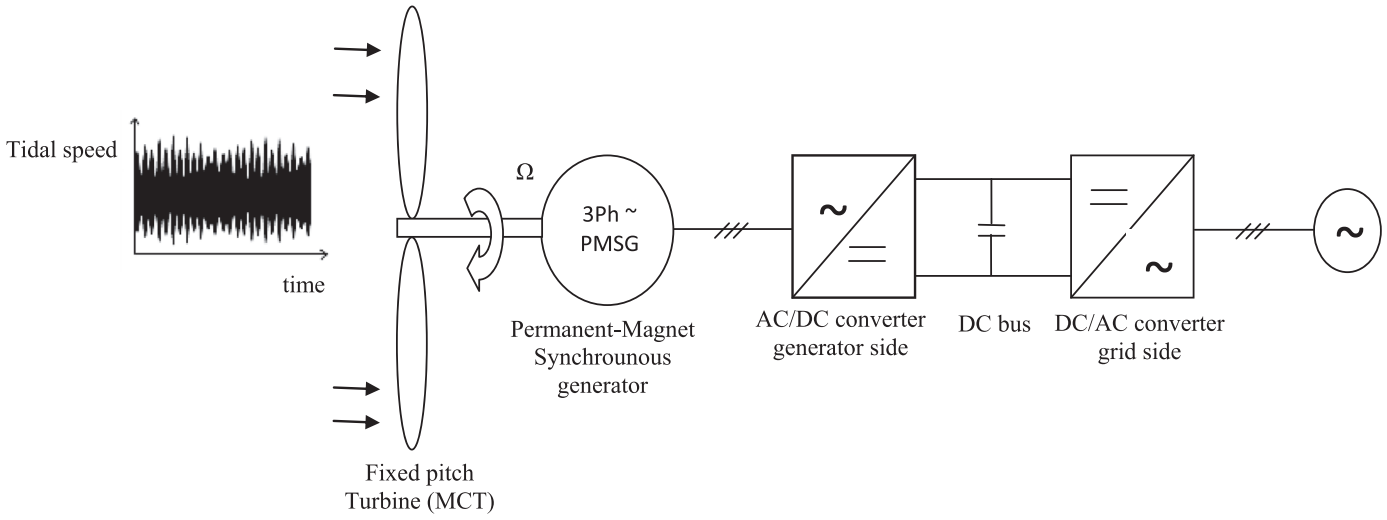

Fig. 1. Marine current turbine drivetrain, direct-drive generator linked to a fixed-pitch turbine.

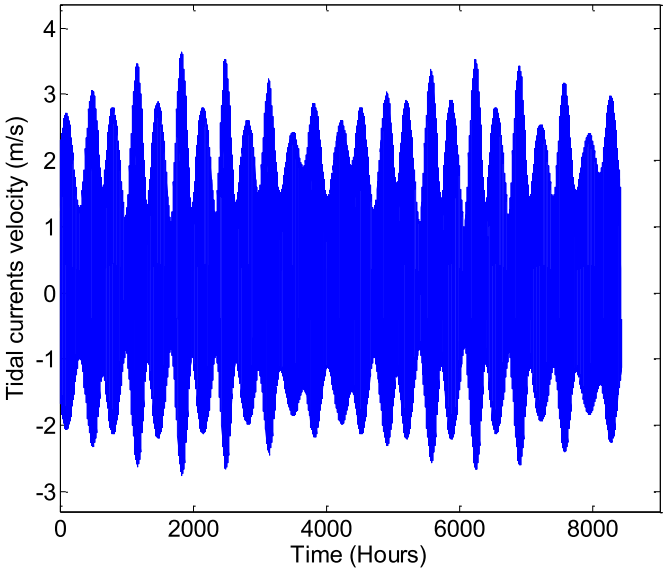

Fig. 2. Tidal currents velocity in Raz de Sein tidal site.

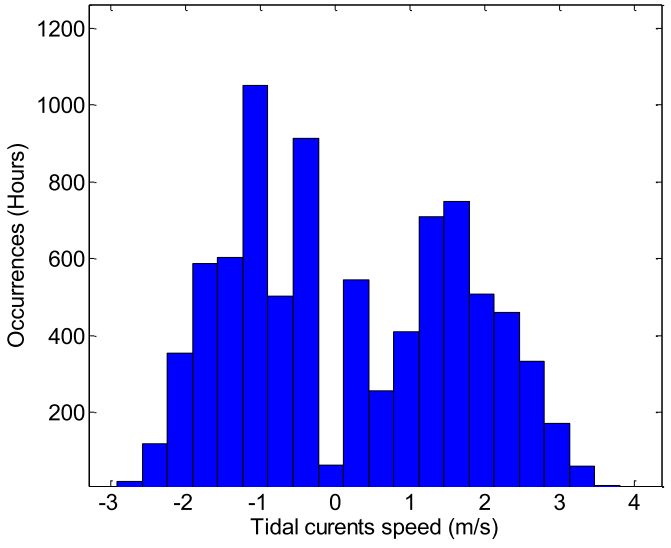

Fig. 3. Occurrences (OCC_i) versus tidal currents velocity (v_i).

performed using the basic relation (2).

$$E^i(v_i) = E^i_{kinetic}(v_i) \times A_{turbine} \times C_{p\max}. \quad (2)$$

The total extractible energy (E_t) during a tidal cycle is obtained by

$$E_t = \sum E^i(v_i). \quad (3)$$

2.2. Turbine modeling

The used hydrodynamic model is a basic quasi-static model of a single turbine (transient phenomena and interaction of several turbines in a farm configuration are not considered is this study). As for wind, tidal turbines are characterized by their C_p (power coefficient) law for a given-steady state point. For fixed-pitch turbines, the C_p characteristic is given as a function of the tip-speed-ratio (TSR) λ, which is defined as the ratio between the blades peripheral speed to the tidal current speed (4).

$$\lambda = \frac{\Omega \times (D_{turbine}/2)}{|v|}. \quad (4)$$

Where Ω (rad/s) is the generator shaft rotational speed, $D_{turbine}$ (m) is the turbine diameter and v (m/s) is the tidal current velocity. In this study, a C_p law of an experimental underwater turbine small scale prototype is used [22]. C_p characteristic data given in [22] is then used. These experimental data are fitted by an analytical law, which is given by (5).

$$\begin{cases} C_p(\lambda) = 0.0195\lambda^2\left(1.3172e^{(-0.3958\lambda+1.539)}\right. \\ \quad \left. -0.0867\cos(0.4019\lambda - 5.6931)\right) \\ \lambda \in [0 \quad 11.8] \end{cases}. \quad (5)$$

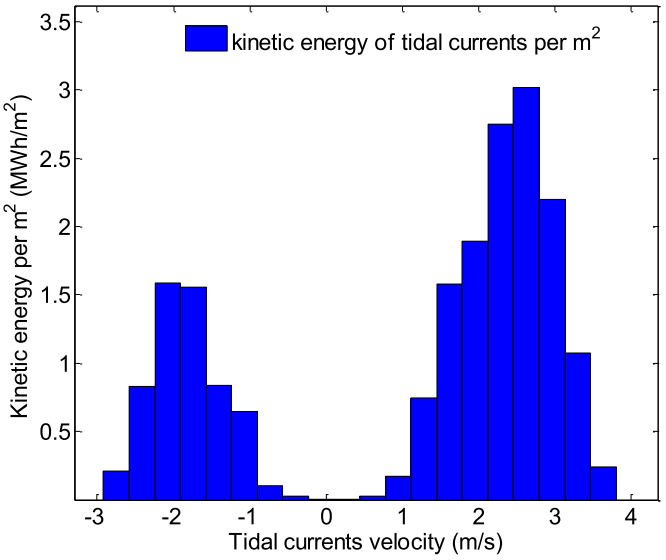

Fig. 4. Tidal kinetic energy distribution per m^2 in Raz de Sein site, France.

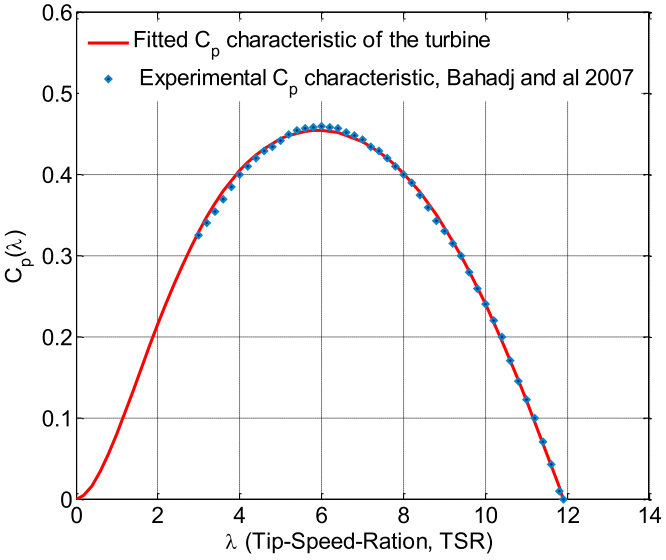

Fig. 5. C_p law characteristic of the considered turbine.

As shown in Fig. 5, the calculated C_p curve with the proposed analytical interpolation law matches with the experimental C_p curve issued from [22].

It is supposed in this work that the considered turbine has a diameter $D_{turbine} = 12\,\text{m}$ and starts operating when tidal currents velocity exceeds 1 m/s, these tidal currents value is denoted v_s. The considered turbine has a maximum power coefficient $C_{pmax} = C_p(\lambda_{opt}) \approx 0.46$ given for an optimal TSR $\lambda_{opt} \approx 6$.

2.3. Control strategy

In this section, the turbine control strategy is defined by considering tidal currents velocity characteristic and the turbine specifications. For each given values of Ω and v, the

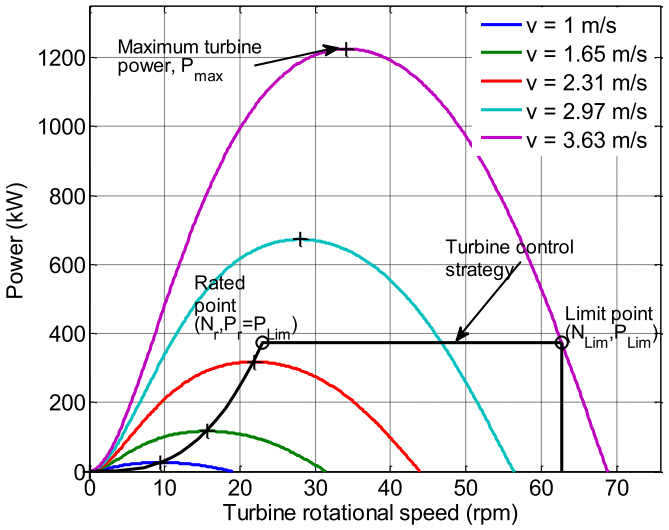

Fig. 6. Extracted power and used control strategy.

turbine extracted power can be calculated by (Fig. 6).

$$P_{turbine} = \frac{\pi}{8}\rho_{water} D_{turbine}^2 C_p(\lambda)\left|v^3\right|. \tag{6}$$

From Fig. 4, it is clearly underlined that tidal currents energy is very small at high tidal currents velocity. It is then obvious that using limitation power strategy is necessary to avoid a significant power oversizing of the electrical conversion chain. It can be also observed from Fig. 4 that tidal currents energy is also very small at low tidal currents velocity. This observation implies that operating at low tidal currents velocity is not relevant in terms of extracted energy quantity. Among tidal currents velocity where turbine starts operating (v_s) and tidal currents velocity where the turbine power is limited (v_r), a maximum power point tracking strategy (MPPT) is considered in order to maximize the extracted energy quantity. Summarizing these turbine power control considerations allows to obtain P^* that represents the reference operating power of the turbine (control strategy). This turbine power reference P^* is determined by (7), see Fig. 6.

$$P^* = \begin{cases} 0 & \text{if} \quad 0 < |v| < v_s \\ \dfrac{\pi}{8}\rho_{water} D_{turbine}^2 C_{pmax}\left|v^3\right| & \text{if} \quad v_s \le |v| < v_r \\ P_{Lim} & \text{if} \quad |v| \ge v_r. \end{cases} \tag{7}$$

P_{Lim} is the turbine power where limitation power strategy is applied. P_{Lim} allows determining the tidal current velocity v_r, where the limitation power strategy begins to be used. It is calculated by

$$v_r = \sqrt[3]{\frac{P_{Lim}}{\left(\frac{\pi}{8}\rho_{water} D_{turbine}^2 C_{pmax}\right)}}. \quad \text{(m/s)} \tag{8}$$

Then the turbine rated rotational speed (Ω_r) is deduced as

$$\Omega_r = \frac{\lambda_{opt} v_r}{(D_{turbine}/2)}. \quad \text{(rad/s)} \tag{9}$$

The turbine rated rotational speed in rpm is then deduced by

$$N_r = \Omega_r \times \frac{60}{2\pi}. \qquad \text{(rpm)} \qquad (10)$$

Eqs. (8)–(10) allow defining the turbine rated operating point (Fig. 6) characterized by the rated power $P_r = P_{Lim}$, the rated rotational speed N_r, and the tidal currents velocity v_r.

The maximum turbine rotational speed Ω_{Lim} (given at the limit operating point, see Fig. 6) is defined by

$$\Omega_{Lim} = \frac{\lambda_{Lim} v_{\max}}{(D_{turbine}/2)}, \qquad \text{(rad/s)} \qquad (11)$$

and

$$N_{Lim} = \Omega_{Lim} \times \frac{60}{2\pi}, \qquad \text{(rpm)} \qquad (12)$$

where Ω_{Lim} and N_{Lim} are the turbine rotational speeds in rad/s and rpm at the limit operating point (Fig. 6), respectively. λ_{Lim} and v_{max} are the corresponding TSR and maximum tidal currents velocity at this limit operating point. λ_{Lim} is calculated by solving the following nonlinear equation.

$$C_p(\lambda) - \frac{P_{Lim}}{\left(\frac{\pi}{8}\rho_{water} D_{turbine}^2 \left|v_{\max}^3\right|\right)} = 0. \qquad (13)$$

Eqs. (11) and (13) allows determining the limit operating point of the turbine (Fig. 6), which is specified by its power P_{Lim} and its rotational speed N_{Lim}.

Considering the turbine start operating point, the turbine power (P_s) and the corresponding rotational speeds (Ω_s and N_s) at this point are given by relations (14)–(16):

$$P_s = \frac{\pi}{8}\rho_{water} D_{turbine}^2 C_{pmax} \left|v_s^3\right|, \qquad (14)$$

$$\Omega_s = \frac{\lambda_{opt} v_s}{(D_{turbine}/2)}, \qquad \text{(rad/s)} \qquad (15)$$

$$N_s = \Omega_s \times \frac{60}{2\pi}. \qquad \text{(rpm)} \qquad (16)$$

By fully knowing the turbine control strategy (P^*), it is then possible to evaluate the extracted energy for each power limitation value using relation (17).

$$E_{extracted} = \sum_{i=1}^{n} P^*(v_i) \times OCC_i(v_i). \qquad (17)$$

To quantitatively determine the value of the turbine rated power P_r (P_r corresponds to the power limitation value P_{Lim}), calculations of the extracted energy are achieved with considering various values of P_{Lim}. P_{Lim} is here varying from 5% to 100% of the maximum power that can be extracted by the considered turbine ($P_{max} = P(C_{pmax}, v_{max}) = 1245$ kW in the studied case). Thereby, Fig. 7 is obtained. It gives the percentage of extracted energy for each values of the power limitation level, according to the used turbine and tidal site.

Increasing the turbine power limitation value P_{Lim} (turbine rated power) will considerably increase the conversion chain

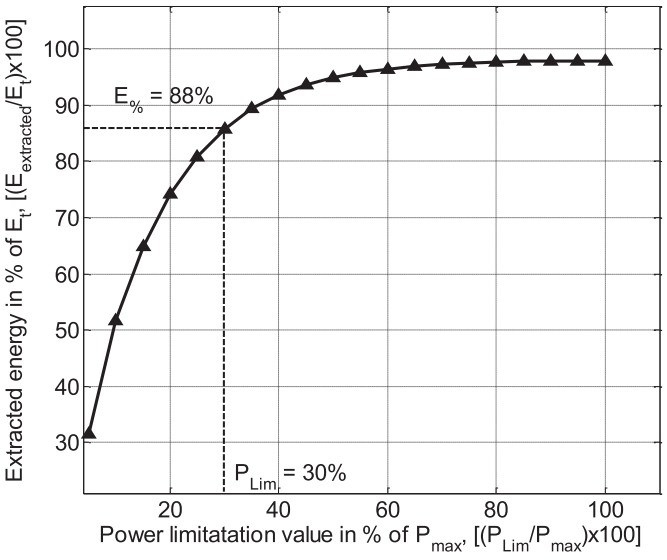

Fig. 7. Extracted energy rate variation versus the power limitation value.

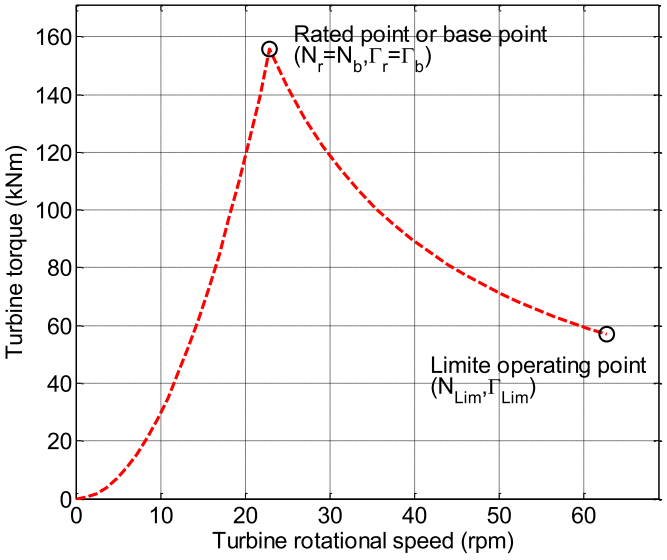

Fig. 8. Turbine/generator torque reference specification.

costs (generator, inverters, cable, etc.) even if the extracted energy is improved. Regarding Fig. 7, the power limitation value can be fixed by choosing a good compromise between the extracted energy and the limitation power value. In our study case, Fig. 7 clearly shows that limiting the turbine power to 30% of its maximum power is enough to extract 88% of total allowable energy in the considered tidal site. Thus, the limitation power value is here set to $P_{Lim} = 374$ kW (30% of P_{max}).

If $P^*(N)$ is quantitatively determined, the reference torque vs. speed characteristic () of the turbine can be deduced from relation (19).

$$\Gamma^*(N) = \frac{P^*(N)}{N \times (2\pi/60)}. \qquad (18)$$

$\Gamma^*(N)$ is given in Fig. 8. If the mechanical losses are neglected, the turbine reference torque can be assimilated to the

generator torque reference. It implies that the turbine power is assumed to be equal to the generator electromagnetic power (P_{EM}). In this paper, it is proposed to control the fixed-pitch turbine power (including power limitation) by using torque control of the generator with considering flux-weakening operation when the generator speed is over the base one. To achieve this strategy, the generator should be able to develop the required torque characteristic $\Gamma^*(N)$ during the operating speed cycle. This characteristic is then introduced as a design specification of the PM generator. It can be observed from Fig. 8 that the design torque characteristic can be introduced to the generator design process as two design points. The first one is the rated design point (generator base point) where the generator must develop the rated torque Γ_r (it corresponds to the generator base torque Γ_b) at the rated rotational speed N_r (it corresponds to the generator base speed N_b). The second one is an over-speed limit point. This point is introduced as a constraint in the generator design specifications. It traduces the torque Γ_{Lim} that the generator should be able to develop at maximum turbine rotational speed N_{Lim} during generator operation speed cycle.

2.4. Power converter limits

During over base speed operation, the generator voltage is limited by the converter voltage limit (V_{max}). Furthermore, the converter cost is directly related to the generator power factor. The rated power of the converter is then equal to $S_{converter} = P_r/PF$, where P_r is the generator rated power and PF is its power factor. When the generator power factor is low the converter rated power increases, which consequently increases the converter cost. In our methodology, the power converter constraints are taken into account. Firstly, the converter is considered as a double-bridge IGBT back-to-back converter [16]. Thus, the grid-side converter voltage is set to $V_{grid} = 690$ V (rms value). Then the maximum generator phase voltage (rms value) allowed by the converter in the generator side is here set to $V_{max} = V_{grid}$. Secondly, the generator power factor is set to 0.81 to avoid a significant oversizing of the converter.

2.5. Generator design

2.5.1. Generator modeling

In this study, a radial flux permanent magnet generator is considered. In order to determine this generator geometry, an analytical magnetostatic electromagnetic model coupled with a thermal one has been used in an optimization process, these models are detailed in [8,10,23,24]. In addition, these models allow evaluating the generator performances as the electromagnetic torque, electrical power, Joule and iron losses, power factor, and the thermal behavior. The generator main dimensions (one pole pair is represented) are illustrated in Fig. 9. This figure shows some of the geometrical variables, which have to be determined in order to evaluate the studied generator designs. These dimensions are also given in Table 2. For this study, the considered generator winding topology is a

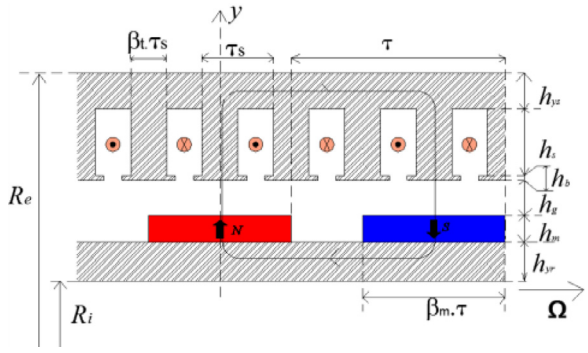

Fig. 9. Geometry of the RFPM generator, R_e is the outer magnetic radius, R_i is the inner magnetic radius, h_{yr} is the rotor yoke height, h_m is the magnet height, h_g is the air gap height, h_s is the slot height, h_{ys} is the stator yoke height, β_m is the magnet-to-pole width ratio, τ_s is the slot pitch width, β_t is the tooth-to-slot width ratio.

basic "one slot per pole and per phase" winding design. Considering this classical winding topology, the winding factor is assumed to be one. However, more sophisticated winding design can be considered introducing a winding factor in the models presented in [8,10,23,24]. By using these models, the generator performances can be evaluated over the operating speed range.

2.5.2. Formulation of the generator design process as an optimization problem

The generator design is formulated as a constrained optimization problem that aims to minimize under constraints the total active parts cost function $C(\mathbf{x})$, where $\mathbf{x}$ denotes here the geometry variables (Fig. 9). The considered constraints are:

- Equality constraint on the generator torque $\Gamma(\mathbf{x},\Omega_r)$ at the rated rotational speed. This constraint is noted Γ^*_r (obtained from Fig. 8) and it corresponds to the generator base speed.
- Equality constraint on the generator phase voltage $V(\mathbf{x},\Omega_r)$, which is defined at the base speed. This constraint is noted V_{max} and it is related to the power converter voltage limit on the generator side.
- Inequality constraint on the generator torque at the limit operating speed, it is mainly used to ensure the turbine power limitation control using the generator, which must develop the required torque over all the operating range. Thereby the generator torque $\Gamma(\mathbf{x},\Omega_{Lim})$ at the turbine maximum rotational speed Ω_{Lim} must be higher than the required torque at this speed Γ^*_{Lim} (obtained from Fig. 8).
- Inequality constraint on the power factor PF. The power factor $PF(\mathbf{x},\Omega_r)$ at the base speed must be higher than the fixed minimal power factor value PF_{min}. This constraint is introduced to avoid design of a generator with a very low power factor.
- Inequality constraint on the generator electrical efficiency. The generator electrical efficiency $\eta_{elec}(\mathbf{x},\Omega_r)$ must be higher than the minimal required value $\eta_{elec,\min}$. This constraint is introduced into the design process to avoid a low generator electrical efficiency.

Table 1
Generator constraints.

Symbol	Definition	Value	Unit
$D_{generator}$	Generator external diameter	3	m
Γ_n	Turbine rated torque	155.6	kNm
N_n	Turbine rated speed	22.95	rpm
Γ_{Lim}	Turbine torque at maximum speed	5.7	kNm
N_{Lim}	Turbine limit speed	62.73	rpm
v_{Lim}	Tidal speed at base point	2.45	m/s
V_{max}	Power converter voltage	690	V(rms)
PF	Generator power factor	0.81	–
$\eta_{elecmin}$	Minimal generator electrical efficiency	96	%
T_{max}	Maximum generator temperature	100	°C
H_{cj}	Magnets coercive field	10^6	A/m

- Inequality constraint on the maximum slot temperature. This constraint ensures the thermal feasibility of the generator. It is defined as the maximum slot temperature $T_{slot}(\mathbf{x},\Omega_r)$ in slots at the rated speed (generator base speed). The temperature $T_{slot}(\mathbf{x},\Omega_b)$ should be lower than the maximum temperature T_{max} allowed by the conductors class thermal insulation.
- Inequality constraint on the maximum magnetic field $H_{max}(\mathbf{x})$ in magnets. The magnetic field in magnets is calculated by considering the worst case where the field created by stator currents is in phase with the magnets field. This assumption utilized on the calculation of the magnets magnetic field allows avoiding the magnets demagnetization over all the speed operating range. Then, the value of magnetic field should be lower than the magnets magnetic coercive field H_{cj}, which is used as a constraint during the optimization process.
- Finally, linear inequality constraints are imposed on the geometry generator variables ($\mathbf{x}$). They are introduced in the optimization problem to ensure the geometry feasibility of the PM generator.

Regarding the formulated optimization variables, objective function, and constraints, the optimization design problem is summarized as

$$\mathbf{x}^* = \min_{\mathbf{x}\in\mathbf{X}} \|C(\mathbf{x})\| \quad \begin{cases} \Gamma(\mathbf{x},\Omega_r) - \Gamma_r^* = 0 \\ V(\mathbf{x},\Omega_r) - V_{\max} = 0 \\ -\Gamma(\mathbf{x},\Omega_{\mathrm{Lim}}) + \Gamma_{\mathrm{Lim}}^* \le 0 \\ -PF(\mathbf{x},\Omega_r) + PF_{\min} \le 0 \\ T_{slot}(\mathbf{x},\Omega_r) - T_{\max} \le 0 \\ |H_{\max}(\mathbf{x},\Omega_r)| - |H_{cj}| \le 0 \\ -\eta_{elec}(\mathbf{x},\Omega_r) + \eta_{elec_{\min}} \le 0 \\ LB \le \mathbf{x} \le UB \end{cases} \tag{19}$$

3. Design results and analysis

3.1. Electromagnetic design and analysis

Table 1 gives the input set parameters introduced as constraints in the design calculation. Thereby generator geometry is obtained as an output of the design procedure. The geometry dimensions are given in Table 2. The electrical parameters and the main performances of the sized generator are calculated and summarized in Table 3. Finally, the designed generator active parts are illustrated by Fig. 10. It can be noted that the torque ripple level (which can be a significant feature for the generator turbine mechanical association) has been evaluated numerically by 2D finite elements analysis for the proposed design. The torque ripple amplitude is about 10% of the rated torque for the rated point.

Table 2
Designed generator.

Symbol	Definition	Value	Unit
J	Current density	3.05	A/mm^2
A_L	Electrical load	50,671	A/m
B_1	First harmonic of the Air gap flux density	0.65	T
p	Pair pole number	68	–
ncd	Number of conductors in series Per slot per phase	5	–
m	Phase number	3	–
S_{pp}	Slot number per pole per phase	1	–
k_f	Slot fill factor	0.5	–
k_{b1}	Winding coefficient given at first harmonic	1	–
R_i	Inner radius	1.35	m
R_e	Outer radius	1.464	m
R_s	Stator bore radius	1.376	m
L_m	Active length	51.7	cm
β_m	Magnet to pole width ratio	66	%
β_t	Teeth pitch ratio	53.9	%
h_{ys}	Stator yoke thickness	1.35	cm
h_{yr}	Rotor yoke thickness	1.35	cm
h_s	Slot height	7	cm
h_b	Slot closure height	4	mm
β_{sc}	Relative slot closure	50	%
h_m	Magnet height	6.88	mm
h_g	Air-gap thickness	5.4	mm

Table 3
Generator characteristic.

Symbol	Definition	Value	Unit
E_1	Phase electromotive force (*emf*)	580.5	V (rms)
V	Phase voltage	690	V (rms)
X_s	Synchronous reactance	1.88	Ohm
L_s	Synchronous inductance	11.5	mH
r_s	Phase resistance	0.1	Ohm
$cos\varphi$	Power factor at base speed	0.81	–
η_{elec}	Generator efficiency	96	%
T_{coils}	Maximum temperature in coils	56	°C
H_{max}	Maximum magnetic field in magnets	0.54	MA/m
P_J	Joule losses at base speed	13.2	kW
P_{fer}	Iron losses at base speed	1.77	kW

3.2. Generator ability in a speed cycle range

Figs. 11 and 12 shows that the generator torque/ and power/speed characteristics are over the specified characteristics (same curves as in Figs. 6 and 8). This result implies that the electrical power limitation strategy at high tidal speed can be performed only by controlling the designed generator according to the given methodology.

According to this control strategy the turbine will operate until 4960 h with MPPT control and 639 h in power limitation

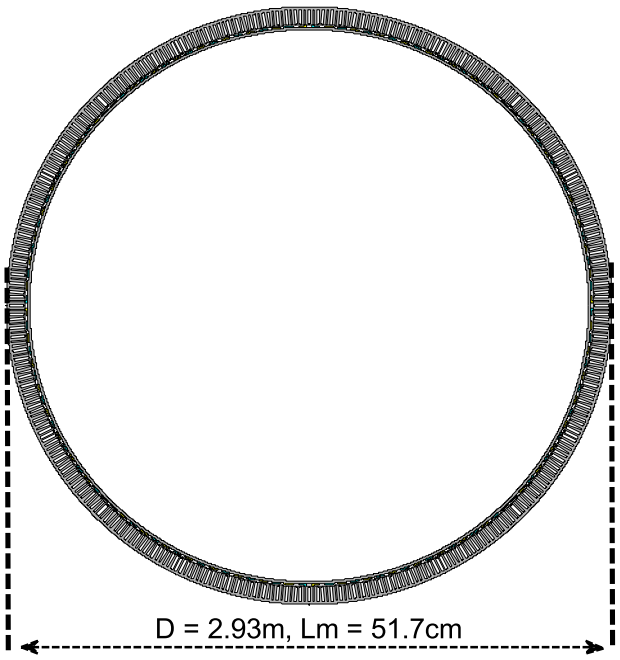

(a)

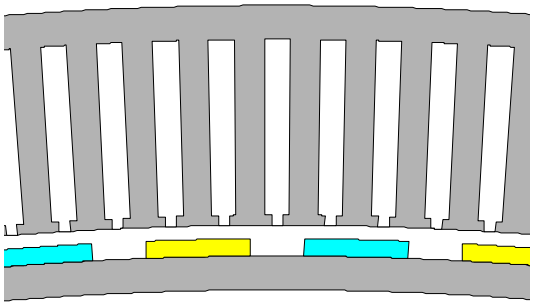

(b) Zoom.

Fig. 10. View of the designed generator active parts.

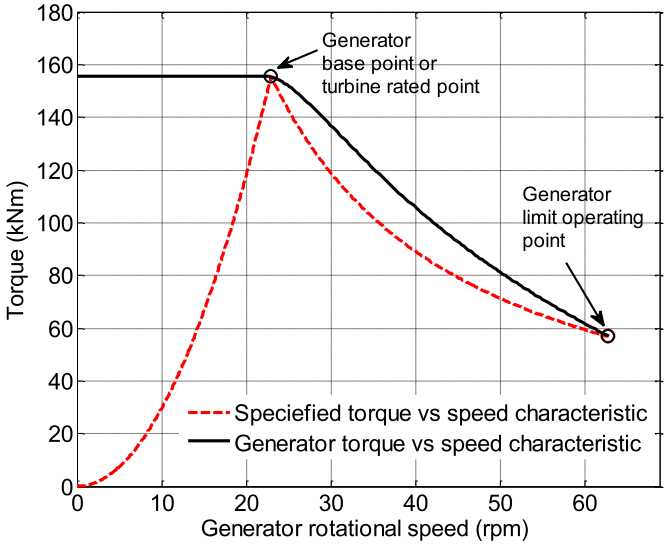

Fig. 11. Required torque/speed specification and generator torque/speed characteristic.

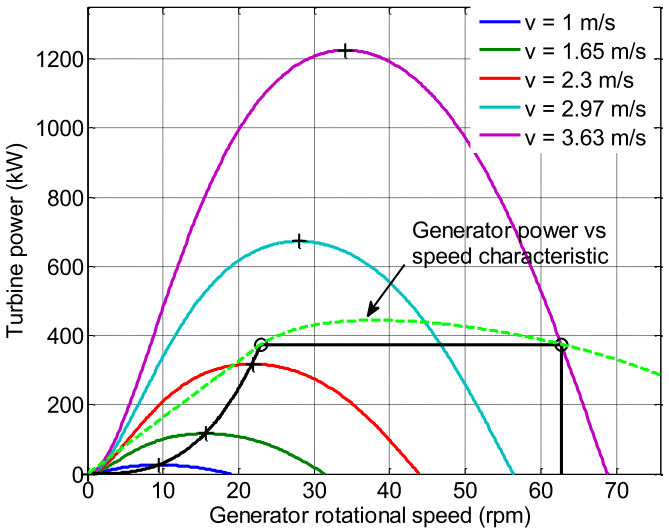

Fig. 12. Power control strategy and developable generator power.

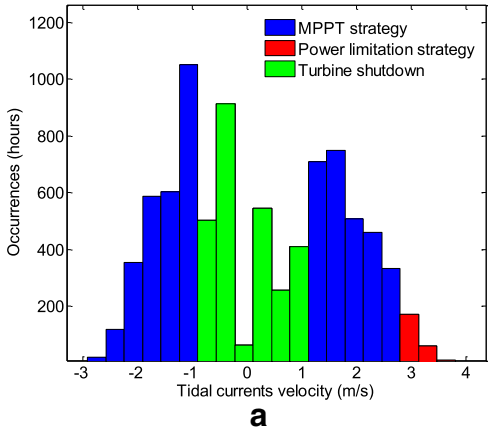

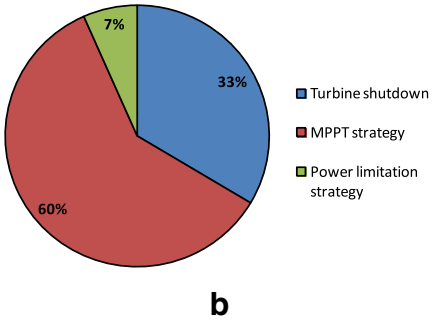

Fig. 13. Occurrences (OCC_i) of each control strategy versus tidal velocity (v_i) (a), repartition of the operating time of each control strategy (b).

mode (Fig. 13(a)). It can be noticed that during 2825 h the turbine is shutdown (Fig. 13(a)). Fig. 13(b) shows that during 60% of the turbine operating time an MPPT control is used while the limitation strategy is used only during 7% of the operating time. In addition the shutdown corresponds to 33% of the operation time.

Fig. 14(a) and (b) shows that 612 MWh (65%) from the total extractable energy (985 MWh) is extracted during the MPPT control mode when 239 MWh (23%) are extracted

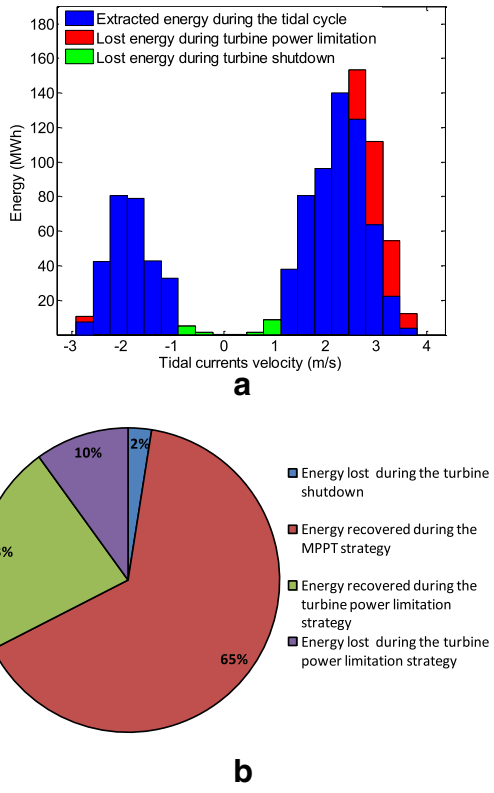

Fig. 14. Energy distribution given for each employed control strategy (a). Extracted energy during for each employed control strategy (b).

during the power limitation control. In this particular case, 113 MWh (10%) are not recovered because of power limitation. The recovery of this clipped energy during power limitation would require tripling the sizing power of the electromechanical conversion chain.

This result shows how it is relevant to limit the turbine power during high tidal currents. Even the turbine is shutdown during 33% of the total operating time, the corresponding energy, which is not recovered, is only 21 MWh (2% of the total energy). According to our considered tidal site and study case, the tidal turbine has a charge rate of 28%, which is corresponding to 2388 h of operation at the rated power. This tidal site is close in term of charge rate to wind turbine sites.

In order to achieve the power control strategy during the turbine operation, the i_q current is controlled to meet the reference torque Γ^* (Fig. 11). This control allows obtaining the turbine power operation characteristic (Fig. 6). The generator reference current $i_{q\text{-}ref}$ is then calculated by (20), where Φ_m is the magnets flux and p the generator pair poles number.

$$\begin{cases} i_{q-ref}(N) = \dfrac{\Gamma^*(N)}{3p\phi_m} & \text{if } N \le N_b \\ i_{d-ref}(N) = 0 & \\ i_{d-ref}(N) = \frac{\phi_m}{L_S} - \sqrt{\left(\frac{V_{max}}{L_S pN\left(\frac{2\pi}{60}\right)}\right)^2 - i_{q-ref}^2(N)} & \text{if } N > N_b \end{cases} \quad (20)$$

According to Table 3, iron losses are very low compared to Joule losses. For this reason a minimal Joule losses control strategy is suitable for low speed marine generators. To achieve a minimal Joule losses strategy the reference current $i_{d\text{-}ref}$ is set to zero below the generator base speed generator (N_b). Over the base speed $i_{d\text{-}ref}$ is calculated by (20) to ensure the generator flux-weakening to maintain the voltage below the converter voltage limit (V_{max}). Parameters of (20) are defined in Tables 1 and 3. Using this equation and the generator given parameters, the reference currents are calculated and illustrated by Fig. 15. Considering these reference currents ($i_{q\text{-}ref}$ and $i_{d\text{-}ref}$), Joule and iron losses curves are then obtained and illustrated by Fig. 16. This figure shows that Joule losses are still very high then the iron ones over all the operating speed range. Fig. 17 gives the generator electrical efficiency over a tidal cycle. It clearly shows that the efficiency is still closer to 96% (electrical efficiency at rated power) over all speed operation range. According to this fig-

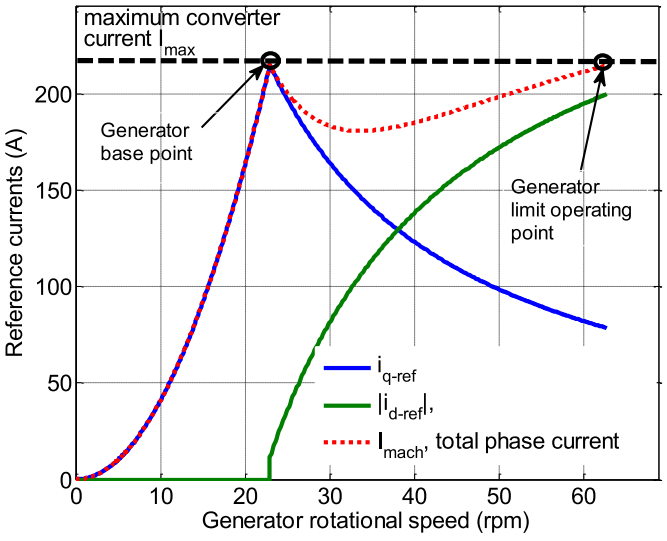

Fig. 15. Generator reference currents leading to minimum Joule losses.

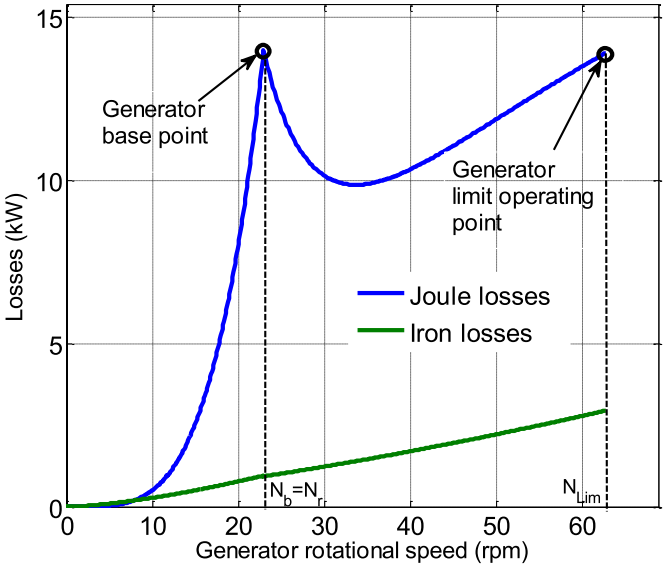

Fig. 16. Generator Joule and iron losses.

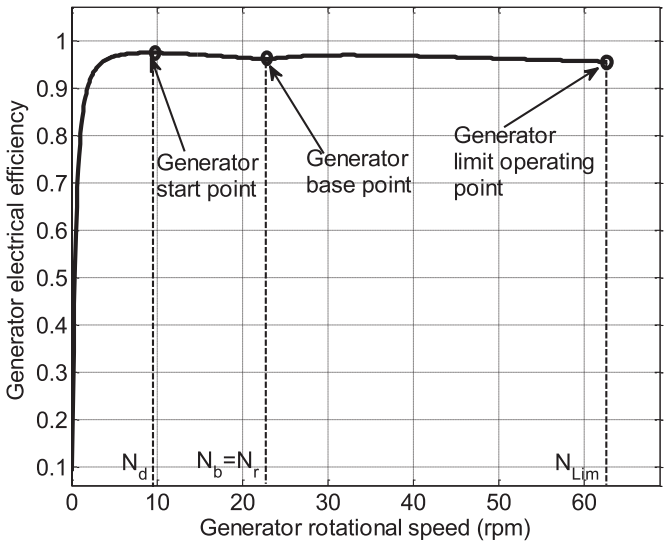

Fig. 17. Generator efficiency during tidal cycle operation.

ure, the electrical efficiency takes its minimal value at the limit operating points. However, the generator efficiency at this limit point (0.957) remains closer to its rated value.

4. Conclusion

Fixed-pitch turbine associated with a direct-drive PM generator seems to be a very attractive solution to increase a tidal turbine reliability, which is an important requirement due to the issues of immersion and offshore location. However, using fixed-pitch turbines implies to use only power converter control for power limitation operations instead of pitch control, which is classically used for high power wind turbines. In this context, this paper has presented a systemic design methodology of direct-drive permanent magnets generator associated to fixed-pitch turbine for tidal generation. The used control strategy used is based on the power limitation at high tidal currents speed by overspeed operations. The proposed power limitation strategy is only based on the flux-weakening control of the generator at high tidal velocities. The given design methodology takes into account the main elements of the conversion chain as: the resource characteristic, the turbine *Cp* law, the generator specifications, the control strategy and the converter constraints. It allows determining the torque/speed characteristic as a design specification of the generator. The obtained results have shown that the designed generator fulfills the required torque characteristic over the speed range and that the proposed solution seems really suitable with the system specifications. Therefore the limitation power at high tidal speed can be achieved without using a variable-pitch system. Considering the designed generator, an energetic analysis of the turbine has been carried out. This analysis has shown the tidal turbine main operation properties. Finally the control strategy with the calculation of the generator currents was given. The obtained results have shown that minimal Joule losses are suitable for tidal applications. It has also been shown that the generator efficiency remains very close to the rated operation efficiency value during all the speed operation range.

Appendix

Tidal Site Characteristics (Raz de Sein)

Tidal velocity (m/s)	Occurrences (h)	Extractible energy (MWh), $C_{pmax}=0.452$, $D_{turbine}=12$m
−2.749	20	10.812
−2.413	118	42.158
−2.077	353	82.371
−1.742	588	80.858
−1.406	603	43.619
−1.070	1052	33.565
−0.734	502	5.177
−0.398	913	1.507
−0.063	63	0.000
0.272	545	0.287
0.608	256	1.500
0.944	410	8.979
1.280	709	38.683
1.615	749	82.200
1.951	509	98.425
2.287	460	143.214
2.623	334	156.832
2.959	170	114.570
3.294	60	55.824
3.630	10	12.448
Total	**8424**	**1014.029**

References

[1] M.E.H. Benbouzid, H. Titah-Benbouzid, Z. Zhou, Encyclopedia of Sustainable Technologies, Elsevier, 2017, pp. 73–85.
[2] M. Melikoglu, Ocean Eng. 148 (2018) 563–573.
[3] F. O'Rourke, F. Boyle, A. Reynolds, Renew. Sustain. Energy Rev. 14 (3) (2010) 1026–1036.
[4] S. Sheth, M. Shahidehpour, in: Proceedings of the IEEE 2005 PPES GM, San Francisco (USA), 2005, pp. 630–635.
[5] N. Maslov, D. Brosset, C. Claramunt, J.F. Charpentier, Int. J. Geo-Inf. 3 (2) (2014) 781–799.
[6] M.E.H. Benbouzid, J.A. Astolfi, S. Bacha, J.F. Charpentier, M. Machmoum, T. Maître, D. Roye, Concepts, Modeling and Control of Tidal Turbines, Marine Renewable Energy Handbook, Chap. 8, Wiley, ISTE, Paris, 2011, pp. 219–278.
[7] Z. Zhou, M.E.H. Benbouzid, J.F. Charpentier, F. Scuiller, T. Tang, Renew. Sustain. Energy Rev. 77 (2017) 852–858.
[8] S. Djebarri, J.F. Charpentier, F. Scuiller, M.E.H. Benbouzid, IEEE J. Ocean. Eng. 41 (1) (2016) 56–60.
[9] S. Djebarri, J.F. Charpentier, F. Scuiller, M.E.H. Benbouzid, in: Proceedings of the 2014 IEEE ICGE, Sfax (Tunisia), 2014, pp. 32–37.
[10] S. Djebarri, On modeling and optimal design of permanent magnets synchronous generators for tidal turbines Ph.D. Thesis, University of Brest, 2015.
[11] J. Ribrant, L. Bertling, IEEE Trans. Energy Conversion 22 (1) (2007) 167–173.
[12] Y. Amirat, M.E.H. Benbouzid, E. Al-Ahmar, B. Bensaker, S. Turri, Renew. Sustain. Energy Rev. 3 (9) (2009) 2629–2636.
[13] S. Djebarri, J.F. Charpentier, F. Scuiller, M.E.H. Benbouzid, in: Proceedings of the 2014 IEEE PEAC, Shanghai (China), 2014, pp. 474–479.
[14] K. Touimi, M.E.H. Benbouzid, P. Tavner, Ocean Eng. 170 (2018) 74–88.
[15] O. Keysan, A.S. McDonald, M. Mueller, in: Proceedings of the 2011 IEEE IEMDC, Niagara Falls (Canada), 2011, pp. 1–6.

[16] J.A. Baroudi, V. Dinavahi, A.M. Knight, Renew. Energy 32 (14) (2007) 2369–2385.
[17] Z. Zhou, M.E.H. Benbouzid, J.F. Charpentier, F. Scuiller, T. Tang, Renew. Sustain. Energy Rev. 18 (2013) 390–400.
[18] S. Djebarri, J.F. Charpentier, F. Sculiller, M.E.H. Benbouzid, in: Proceedings of the 2015 EWTEC, Nantes (France), 2015, pp. 1–10. Paper 08A2-2-1.
[19] Z. Zhou, F. Scuiller, J.F. Charpentier, M.E.H. Benbouzid, T. Tang, IEEE J. Ocean. Eng. 40 (3) (2015) 536–545.
[20] V. Mester, F. Gillon, S. Brisset, P. Brochet, in: Proceedings of the 2006 IEEE VPPC, Windsor (UK), 2006, pp. 1–6.
[21] S. Benelghali, R. Balme, K. Le Saux, M.E.H. Benbouzid, J.F. Charpentier, F. Hauville, IEEE J. Ocean. Eng. 32 (4) (2007) 786–797.
[22] A.S. Bahaj, A.F. Molland, J.R. Chaplin, W.M.J. Batten, Renew. Energy 32 (3) (2007) 407–426.
[23] S. Djebarri, J.F. Charpentier, F. Sculiller, M.E.H. Benbouzid, S. Guemard, in: Proceedings of the 2012 IEEE ISIE, Hangzhou (China), 2012, pp. 1450–1455.
[24] L. Drouen, J.F. Charpentier, E. Semail, S. Clenet, in: Proceedings of the 2007 IEEE OCEANS, Aberdeen (Scotland), 2007, pp. 1–6.